

Finite-Element Modeling of the Nonlinear Behavior of Bolted T-Stub Connections

Ana M. Girão Coelho¹; Luís Simões da Silva²; and Frans S. K. Bijlaard³

Abstract: This paper describes a finite element model for the characterization of the nonlinear behavior of bolted T-stub connections that idealize the tension zone of bolted joints. Two different types of T-stub elements are considered: rolled profiles that are cut along the web, and two plates, flange and web, that are welded in a T shape by means of a continuous fillet weld. The results of existing experimental work are used to calibrate the models. It is found that the numerical approach allows the quantitative actual response to be accurately reproduced. In the case of welded T-stubs, the differences between the numerical model and the experiments are greater due to the effects of residual stresses and modified mechanical properties close to the weld toe, which are not easy to quantify. A parametric study is also undertaken to provide insight into the overall behavior, failure modes, and deformation capacity of the various specimens. A proposal for prediction of failure criteria of these simple connections is also presented and discussed.

DOI: 10.1061/(ASCE)0733-9445(2006)132:6(918)

CE Database subject headings: Deformation; Finite element method; Connections, bolted; Stiffness.

Introduction

The rotational behavior of structural joints is inherently nonlinear. Such behavior results from a multitude of mechanisms that include, in the particular case of bolted end plate beam-to-column bare steel connections: (1) web panel zone deformation; (2) column flange and end plate bending deformations; (3) combined tension/bending bolt elongation; (4) beam deformations within the connecting zone; and (5) weld deformations. In the context of the component method (Weynand et al. 1995) these sources of deformability, generally known as joint components, are assembled into a mechanical model made up of extensional springs (components) and rigid links. Each component is characterized by a force-deformation (F - Δ) response. The spring assembly is treated as a structure and the moment-rotation response of the whole joint is derived from the F - Δ behavior of the individual components.

Bolted end plate beam-to-column joints should exhibit large rotation capacity, ideally characterized by initial yielding of the beam(s) and column web panel zone, followed by yielding of the column flange and/or end plate under tension and elongation of

the bolts. In this common case, the joint rotational response is mostly governed by the deformation of the latter components, which form the tension zone of the joint. This zone can be modeled by means of “equivalent T-stubs” (Zoetemeijer 1974; Yee and Melchers 1986) [Fig. 1(a)], which correspond to two T elements connected through the flanges by means of one or more bolt rows. The T elements on the column flange side are in general hot rolled profiles (HR-T-stubs) [Fig. 1(b)] while on the end plate side such elements comprise two welded plates (WP-T-stubs), the end plate and the beam flange, and a further additional stiffener that corresponds to the beam web [Fig. 1(c)].

T-stub connections as a standalone configuration have been widely studied over the past years. The emphasis in most of the research on this subject was mostly placed on the assessment of the connection resistance and stiffness properties (Kato and McGuire 1973; Nair et al. 1974; Zoetemeijer 1974; Packer and Morris 1977; Astaneh 1985; Thornton 1985; Yee and Melchers 1986). Several experimental tests were carried out for the prediction of the F - Δ response (Bursi and Jaspart 1997; Gebbeken et al. 1997; Piluso et al. 2001b). However, these studies were restricted to HR-T-stubs. Piluso et al. (2001b) refer to a single experimental test on WP-T-stubs. The information extracted from those experiments was used for validation of analytical and numerical finite element (FE) methodologies. In particular, regarding the FE analyses, Bursi and Jaspart (1997), Zajdel (1997), and Wanzeck and Gebbeken (1999) all implemented three-dimensional nonlinear models that were able to account for most of the T-stub features, showing a good agreement with the experimental results.

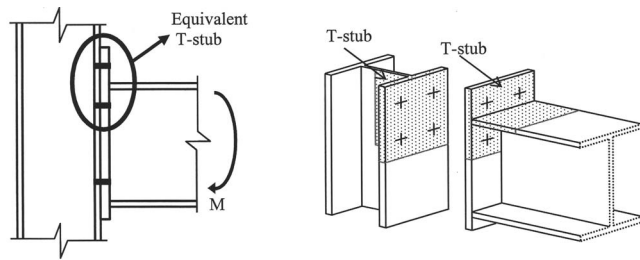
More recently, Swanson (1999) and Swanson et al. (2002) performed several tests on individual T-stubs and implemented a robust FE model to supplement their research. This sophisticated model provided insight into the characteristics of the T-stub behavior and stress distributions (namely, contact stresses) and was compared and calibrated with a single experimental result. The authors explored many features of the T-stub model, such as the bolt response and the prying effect. However, they used nominal properties instead of measured material properties. The results of

¹Research Assistant, Civil Engineering Dept., Polytechnic Institute of Coimbra, Rua Pedro Nunes, 3030-199 Coimbra, Portugal. E-mail: a.m.girao@clix.pt

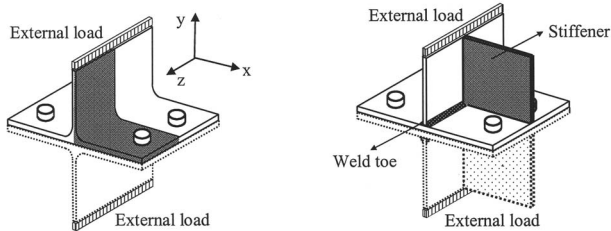
²Professor, Civil Engineering Dept., Univ. of Coimbra, Polo II, Pinhal de Marrocos, 3030-290 Coimbra, Portugal (corresponding author). E-mail: luiss@dec.uc.pt

³Professor, Steel and Timber Structures, Faculty of Civil Engineering, Delft Univ. of Technology, P.O. Box 5048, 2600 GA Delft, The Netherlands. E-mail: f.s.k.bijlaard@citg.tudelft.nl

Note. Associate Editor: Sashi K. Kunnath. Discussion open until November 1, 2006. Separate discussions must be submitted for individual papers. To extend the closing date by one month, a written request must be filed with the ASCE Managing Editor. The manuscript for this paper was submitted for review and possible publication on January 21, 2003; approved on October 17, 2005. This paper is part of the *Journal of Structural Engineering*, Vol. 132, No. 6, June 1, 2006. ©ASCE, ISSN 0733-9445/2006/6-918-928/\$25.00.



a) Unstiffened bolted extended end plate connection: T-stub identification and orientation



b) T-stub model for the column flange side

c) T-stub model for the end plate side

Fig. 1. T-stub identification and representation

this model were used to validate a simpler two-dimensional model.

All FE simulations discussed above were basically aimed at the accomplishment of a reliable FE model, calibrated against experiments to validate the FE response. However, none of the authors used their models to broaden the scope of their analysis (e.g., prying effect) or to determine the mechanisms and parameters that influence the T-stub behavior. Furthermore, those authors did not attempt to bridge the gap between the available (predictive) analytical approaches currently available in terms of code provisions (CEN 2003; AISC 2005) and the experimental evidence. This is particularly true with respect to the evaluation of the ductility of T-stub connections.

Given the essential role of T-stub connections as a controlling part of the behavior of end plate joints, the assessment of the overall deformation response and the description of the basic mechanisms of T-stub behavior in the framework of a numerical FE modeling are the main topics of the paper. A three-dimensional FE model is hence proposed to predict the nonlinear $F-\Delta$ overall T-stub response. The validation of the model is based on experimental data available in the literature for the HR-T-stubs (Bursi and Jaspart 1997) and test results from an experimental program carried out by the authors are used for the WP-T-stubs (Girão Coelho et al. 2004). The model provides insight into the pressure distributions on contact surfaces and, consequently, it affords some basis for a thorough description of the prying effect (evaluation of the prying forces and their location with the course of loading). Additionally, it highlights the main differences between HR-T-stubs and WP-T-stubs. A parametric study is also introduced in order to gain insight into the main differences between both assembly types and to analyze the influence of the key geometrical and mechanical connection parameters. This study also constitutes a database to calibrate simplified models for design purposes, particularly for prediction of the deformation capacity of the connection. Finally, it leads to the proposal of failure criteria for T-stub connections.

Finite-Element Modeling of Isolated Bolted T-Stub Connection

The behavior of a bolted T-stub connection is three dimensional in nature. Such behavior is highly nonlinear, involving complex phenomena such as material plasticity, second-order effects, and unilateral contact boundary conditions. In the following sections, the procedures for the implementation of a FE model using the commercial FE package LUSAS (2000) for the analysis of this type of problem are described.

Description of Model

The T-stub connection is generated with three-dimensional elements, solid, and joint compatible elements. In particular, the solids are hexahedral eight-node bricks (HX8M) and are used to model the continuum. The joint elements (JNT4) are employed in the simulation of element contact. The brick elements belong to a family of serendipity isoparametric elements. The elements have three translational degrees-of-freedom per node and are numerically integrated (full integration, $2 \times 2 \times 2$ Gauss points). The kinematic description of the solid elements in nonlinear geometrical analysis is based on the updated Lagrangian formulation.

For the material nonlinearity, an elastoplastic constitutive law with isotropic strain hardening based on the Von Mises yield criterion is adopted. The constitutive model is integrated by means of the explicit forward Euler algorithm. A true stress-logarithmic strain measure ($\sigma_n - \epsilon_n$) is used for the definition of the uniaxial material response.

Node-to-node nonlinear contact friction elements simulate the interface boundary conditions. The contact between two bodies is modeled with a joint mesh interface, which uses a “master” and “slave” connection to tie the two surfaces together at their nodes. The sliding and sticking conditions are reproduced with the classic isotropic Coulomb friction law. The joint element JNT4 connects two adjacent nodes by means of extensional springs in the three local directions.

To determine the structural response of the nonlinear problem an implicit solution strategy is used, which is suitable for problems involving smooth nonlinear analyses. A load stepping routine is hence used. The increment size follows from accuracy and convergence criteria. Within each increment, the equilibrium equations are solved by means of the Newton–Raphson iteration. The following convergence criteria were used (LUSAS 2000): (1) Euclidean displacement norm (3%); (2) Euclidean incremental norm (3%); and (3) work norm (0.05%). With respect to the incremental method, a load curve is defined. Loads are applied to the specimen in a displacement-control fashion that enforces a better conditioning of the tangent stiffness matrix when compared to the classical load-control procedure.

Calibration of Model with Experimental Evidence

The FE model for both T-stub assembly-types is identical. The only difference lies in the representation of the flange-to-web connection. For the HR-T-stub, flange and web are connected by means of a fillet radius (r) that ensures the continuity between both plates. In the case of WP-T-stubs, a continuous 45° -fillet weld (throat thickness a_w) links the flange and the web, though the two plates are not necessarily in contact.

The calibration of the FE model for the HR-T-stub is based on the experimental test program carried out by Bursi and Jaspart (1997). The specimen T1, which was obtained from an IPE300

Section xx

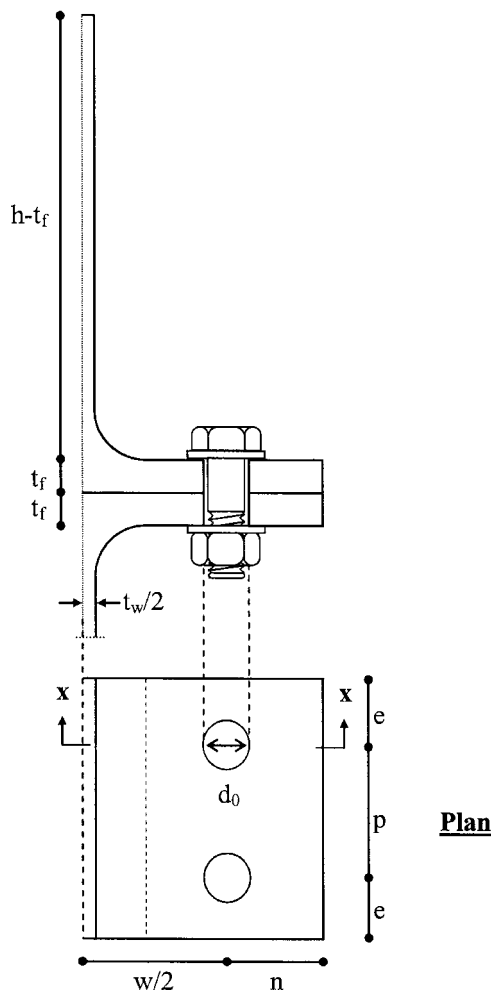


Fig. 2. T-stub specimen general characteristics

beam profile, with snug-tightened bolts is selected for the following study. Regarding the WP-T-stub, the approach is validated with experimental evidence from a series of 32 tests on this type of assembly that were carried out at the Delft University of Technology (Girão Coelho et al. 2004). The specimen WT1 is selected for calibration of the numerical procedure.

Geometry

The geometrical characteristics of the specimens are depicted in Fig. 2 and specified in Table 1 for the two specimens reported herein. By adopting the adequate boundary conditions only one eighth of the T-stub is modelled, owing to symmetry considerations (Fig. 2). The xy and yz planes are geometrical planes of symmetry. Though the xz plane does not meet such a criterion,

since the bolt elongation behavior is not symmetrical along the y direction, some authors (Bursi and Jaspart 1997; Wanzek and Gebbeken 1999) propose numerical models that account for a symmetric behavior of an “equivalent bolt” complying with the requirements for symmetry in the xz plane. The “equivalent bolt” is defined in such a way that its geometrical stiffness is identical to that of the actual bolt, i.e. the elongation of the “equivalent bolt” represents half of the elongation behavior of the actual bolt. The xz symmetry plane between the two flanges is then modeled by contact elements on a rigid foundation. The interface boundaries between the flanges and washer or bolt head, and between web and flange plates in the case of WP-T-stubs, are also modeled by means of contact elements. In order to reduce the number of contact planes, the bolt head or nut and the washer, if any, are assumed fully connected. This simplification leads to slightly stiffer deformation behavior, but the overall response is not greatly influenced, as already shown in the literature (Zajdel 1997; Bursi and Jaspart 1997; Wanzek and Gebbeken 1999).

The bolt modeling must account for the various sources of flexibility: head, nut, and shank (threaded and nonthreaded part). In the proposed numerical model, the “equivalent bolt” has half of the conventional bolt length, L_b , as defined in Eurocode 3 (CEN 2003) and the “equivalent shank” has a threaded part (cross-sectional area A_s) and a nonthreaded portion (actual bolt diameter). The length of these parts is proportional to those of the real bolt.

Boundary and Load Conditions

The nodes in the symmetry planes xy and yz are fixed with symmetric geometrical boundary conditions. The nodes in plane xz between the flange and the rigid foundation and between the washer/bolt head and the flange and between the two plates in the welded assembly are restrained with contact elements, as already pointed out. The nodes on the rigid base are fully restrained. Also, complying with geometrical symmetry, the bottom surface bolt nodes are fixed in the y direction.

Regarding the interface boundary conditions, no friction is assumed between the flanges interface because of the T -elements symmetric behavior. For the flange-washer/bolt head and web flange (WP-T-stubs only) interfaces a friction coefficient, μ , of 0.25 is adopted (Vasarhelyi and Chiang 1967).

A uniform total prescribed displacement of 0.1 mm is applied at the top of the T-element in the positive y direction. In the nonlinear analysis, the total load factor is increased from 1.0 to collapse.

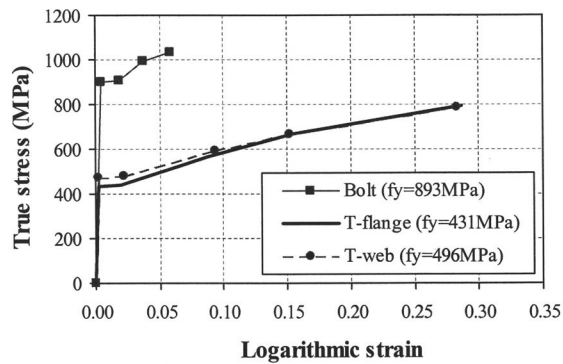
Steel Components Material Properties

For good correlation with experimental results, the full actual stress-strain relationship of the materials must be adopted in the numerical simulation. The constitutive laws are reproduced with a piecewise linear model (Bursi and Jaspart 1997; Girão Coelho et al. 2004)—Fig. 3. The material properties for the rigid

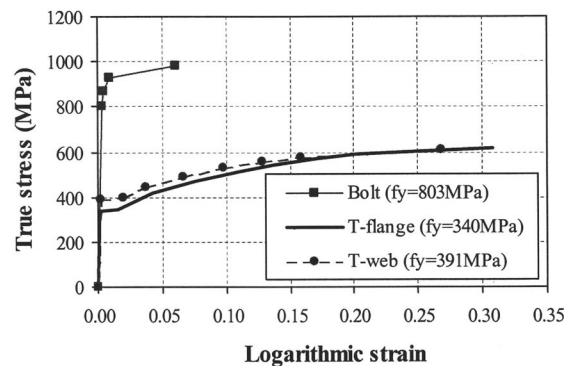
Table 1. Nominal Geometrical Properties of Various Specimens

Test ID	Assembly type	T-elements geometry									Bolt characteristics			
		h (mm)	t_f (mm)	t_w (mm)	w (mm)	n (mm)	$p/2$ (mm)	e (mm)	r/a_w (mm)	d_0 (mm)	ϕ (mm)	Washer (mm)	Type (mm)	Number
T1	Rolled	150	10.7	7.1	90	30	20	20	15	14	12	Yes	ST ^a	4
WT1	Welded	200	10.0	10.0	90	30	25	20	5	14	12	No	ST ^a	4

^aST=short threaded.



(a)



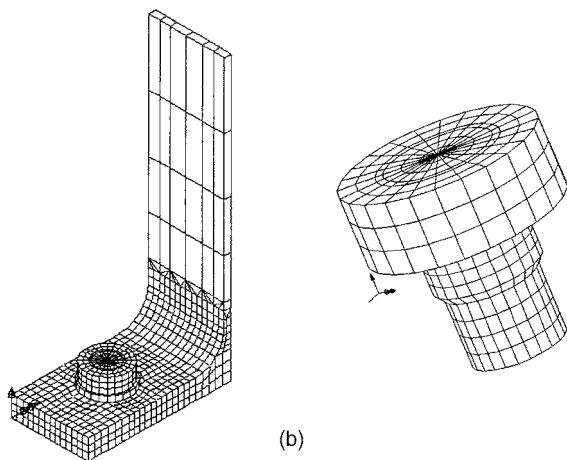
(b)

Fig. 3. True stress-logarithmic strain material laws: (a) HR-T-stub specimen T1 (data adapted from) Bursi and Jaspert 1997; (b) WP-T-stub specimens (Girão Coelho 2004)

foundation are also defined, a linear material being assumed, with a Young modulus, E , of 10^{15} MPa and Poisson's coefficient, ν , of 0.45.

Specimen Discretization

A mesh convergence study with respect to the degree of discretization of the flange, in order to represent the bending dominated problem, and the number of elements through thickness, to check the capability of representing the yielding lines, has been performed within the framework of this research work. The FE mesh depicted in Fig. 4(a) meets the requirements for a reliable



(a)

(b)

Fig. 4. Specimen finite element mesh: (a) global mesh (3,588 elements and 5,680 nodes); (b) bolt discretization

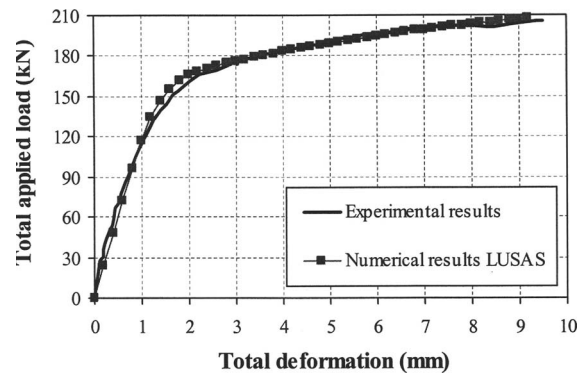


Fig. 5. Global response of specimen T1: numerical and experimental results

simulation and satisfies the convergence study that was carried out. For the bolt discretization, in order to simulate the complex state of stress in the bolt, a reasonably refined mesh is essential. The number of elements is determined decisively by the discretization of the circumference of the bolt. The literature suggests a minimum of 12–16 nodes around the circular hole (Virdi 1999). The bolt mesh represented in Fig. 4(b) also complies with the requests for an accurate modeling.

Failure Criteria

The deformation capacity of a bolted T-stub connection first and foremost depends on the plate strength/bolt strength ratio and eventually is governed by bolt fracture or cracking of the plate material. In both situations, the modeling of the failure condition can be ascertained by assuming that cracking occurs when the ultimate strain ϵ_u is attained, either at the bolt or at the T-element critical sections (Gioncu et al. 2000; Piluso et al. 2001a). Due to the nature of the materials, the available bolt deformation is substantially less than the plate. While for high strength bolts the ultimate strain is $\sim 5\text{--}6\%$, for constructional steels, ultimate strains of 25–30%, at least, can be expected. As a result, bolt fracture is likely to govern most ultimate conditions and its assessment is of primary importance.

The potential failure mechanisms of a bolt under axial loading are: (1) tension failure; (2) stripping of the bolt threads, and (3) stripping of the nut threads. Swanson (1999) points out that high-strength fasteners are designed so that tension failure of the bolt occurs before stripping of the threads. Therefore, the ultimate deformation of the bolt is governed by tension failure. A comprehensive numerical study on the behavior of a single bolt in tension was hence carried out to evaluate its maximum deformation capacity and has been recently reported by Girão Coelho (2004). It has been concluded that since the bolt, as a T-stub element, is subjected to combined tension and bending deformations, failure should be assessed by comparison of the maximum average principal strain, $\epsilon_{11,av.bolt}$ with $\epsilon_{u,bolt}$. Should the flange section be critical, a similar criterion based on the maximum principal strain, i.e., $\epsilon_{11,av.flange} = \epsilon_{u,flange}$, seems appropriate.

Numerical Results for HR-T-Stub T1

The most significant characteristic describing the overall behavior of the model is the load-deformation curve. Fig. 5 compares the actual T-stub behavior with the numerical predictions (the curves include the web deformation). The numerical results are

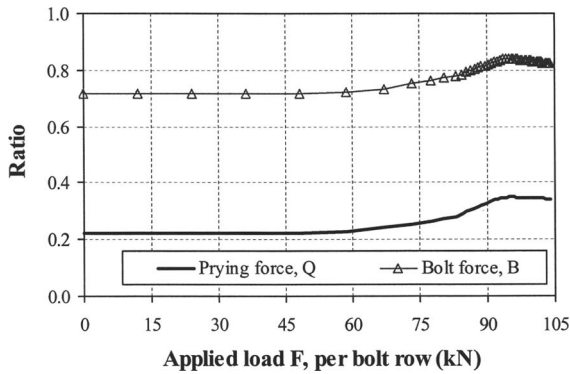


Fig. 6. Numerical results for specimen T1: bolt and prying force

compliant with the experimental response (Bursi and Jaspart 1997) showing that the proposed model is rather accurate. The end of the numerical curve, i.e., the deformation capacity of the connection is established by application of the above failure criterion. For the T-stub specimen T1, experimental observations indicate that the collapse is due to inelastic phenomena in the bolts and significant flange yielding (Bursi and Jaspart 1997). Under the above failure criterion, the ultimate conditions are governed by bolt fracture. The maximum average bolt strain $\varepsilon_{11,av,bolt}$ equals $\varepsilon_{u,bolt}$ for a global deformation of 9.20 mm. This value is very close to the experiments (9.49 mm; ratio=0.97).

Fig. 6 plots the evolution of the ratios of prying and bolt forces with the applied load, per bolt row, F , Q/F and B/F , respectively. It clearly shows the increase of such ratios with plastic straining in the flange. The evolution of the flange yielding is represented in Fig. 7. The yielding of the flange starts at a load level $2F=96$ kN [Fig. 7(a)]. The ratio Q/F for this load level is 0.22. At failure ($2F=208$ kN) it increases to 0.34 (1.5 times larger). This information on the contact pressures provided by the FE model is very useful and cannot be obtained from experiments. Furthermore, the model gives detailed results for the bolt behavior, particularly in terms of bolt elongation behavior.

The location of the prying forces changes during the course of loading. Fig. 8 shows the evolution of the contact area with the applied load. Clearly, as the load increases, the contact area spreads to the bolt axis (Q is shifted inside, from the tip of the flanges).

Numerical Results for WP-T-Stub WT1

Two tests from series WT1 (WT1g/h) are selected for further comparisons (Girão Coelho et al. 2004). Fig. 9(a) compares the

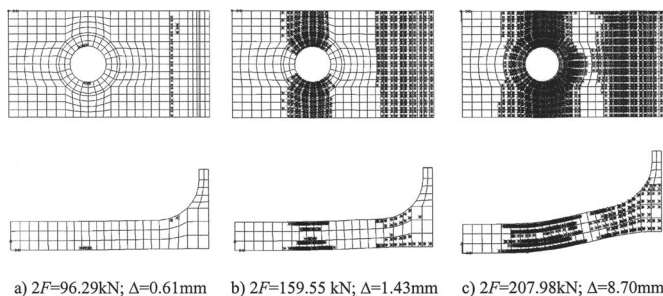


Fig. 7. Flange yielding evolution with applied load

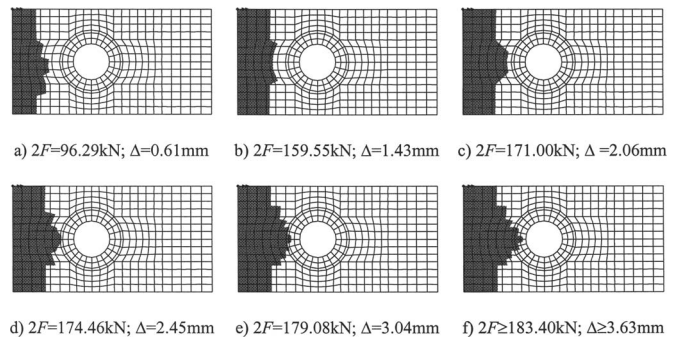
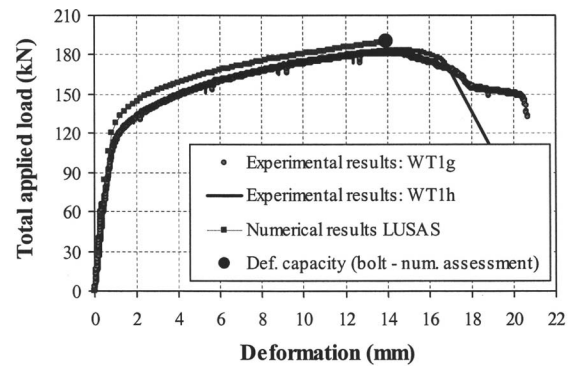


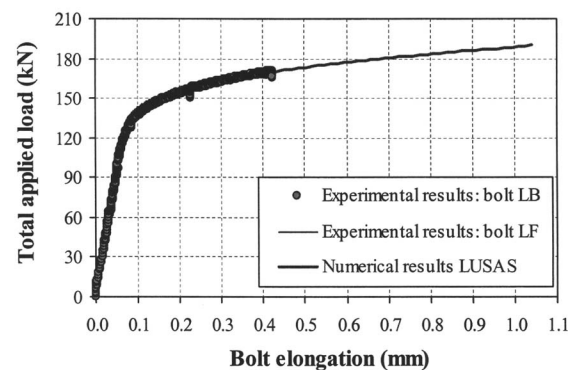
Fig. 8. Evolution of contact area with applied load

load-carrying behavior from the numerical model with the experiments. Fig. 9(b) shows the bolt elongation response for specimen WT1h, for the broken bolts: (LB) left back and (LF) left front. The bolt elongation was carried out by means of a special device that records the deformation directly that was removed prior to collapse.

The FE model yields stiffer results than the experiments, although the agreement is good. The differences may derive from the insufficient geometrical and mechanical characterization of the fillet weld and also because of the modeling of the heat affected zone near the weld toe. In fact, some authors (Piluso et al. 2001b) have already highlighted the fact that due to the welding process, the connection behavior and the cracking of material, in particular, is influenced by the presence of residual stresses and modified microstructure in the heat affected zone. It is very difficult to quantify these effects and therefore they are not included



(a)



(b)

Fig. 9. Global response of specimen WT1: numerical and experimental results: (a) load-deformation behavior; (b) bolt elongation behavior

in the simulations. However, it should be borne in mind that if cracking of material governs the collapse model, a reduction of the ultimate strain with respect to the unaffected material is advised. For both specimens WT1g/h, bolt fracture determines the failure mode. Yet, for specimen WT1g there was a combined failure type involving cracking of the flange in the heat affected zone and bolt fracture. The graph from Fig. 9(a) also shows this type of fracture: at a deformation level of ~ 14 mm there is a smooth drop of load that follows on until fracture of the bolt at 20.5 mm. Numerically and under the above proposed failure criterion, it is established that bolt determines collapse. This is in line with experimental observations and the numerical prediction (13.98 mm) matches the experimental results for WT1h (15.11 mm at maximum load). The average maximum principal strain level in the heat affected zone is 6.8% with a local maximum of 14% (FE results). For the flange plate, the maximum (natural) strain measured in standard material tensile testing is 30.8%.

Regarding the ratio Q/F and the evolution of the location of the prying forces for specimen WT1, their evolution with the external load is identical to the aforementioned for specimen T1 (see Fig. 6). In the elastic regime, $Q/F=0.26$ and at failure, $Q/F=0.37$. There is amplification in Q/F of 1.42 and the prying force shifts to the bolt vertical axis as the load increases.

Parametric Study

Description of Specimens

In order to identify the dependence of the T-stub behavior on the main geometrical and mechanical variables a numerical FE parametric analysis is undertaken. For the WP specimens, two series without stiffeners and with parallel webs are chosen from the whole experimental program (Series 4A and 7—Girão Coelho et al. 2004). Three supplementary WP-T-stubs derived from HR-T-stub T1 are also considered to compare the behavior of the two assembly types. The main geometric parameters that are varied in the study are: (1) gauge of the bolts, w ; (2) pitch of the bolts, p ; (3) distance between the bolt axis and the tip of the flanges, n ; (4) edge distance, e ; (5) flange thickness, t_f ; (6) bolt diameter, ϕ ; and (7) thread length of the bolt and (8) bolt pre-loading, S_0 . The steel constitutive law is the mechanical variable in the study. Additionally, the question of the number of bolt rows is also tackled. The main characteristics of the several specimens are summed up in Girão Coelho (2004).

In the following sections the numerical load-carrying behavior of several specimens is compared to assess the influence of the main parameters.

Influence of Assembly Type and Weld Throat Thickness

The influence of welding and the size of the fillet weld on the overall behavior is analyzed in this section. The equivalent WP-T-stub (generally labeled Weld_T1 hereafter) is identical to T1 in terms of geometrical and mechanical properties. The flange-to-web connection radius is thus replaced with a continuous 45° fillet weld of throat thickness: (1) $a_w=0.5t_w=3.55$ mm [Weld_T1(i)]; (2) $a_w=t_w=7.10$ mm [Weld_T1(ii)]; and (3) $a_w=10.00$ mm [Weld_T1(iii)]. The values for a_w are chosen to meet the Eurocode 3 (CEN 2003) requirements. The first value, $a_w=0.5t_w$, complies with the minimum dimension prescribed in

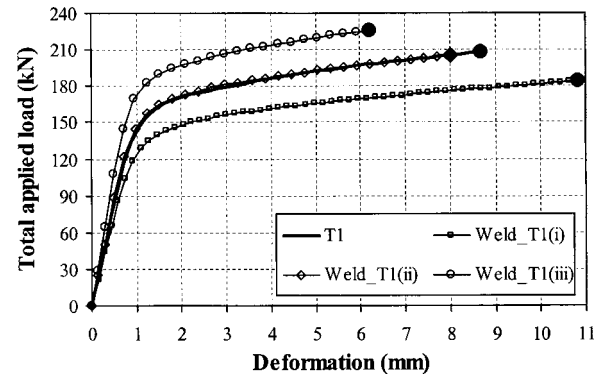


Fig. 10. Overall response of specimens T1 and Weld_T1

the code (3.0 mm), and is commonly used in practice. The value $a_w=t_w$ can be regarded, in design practice, as an upper value for the size of the fillet weld. Finally, the latter value yields a similar distance m (distance between the bolt axis and the critical section at the flange-to-web connection, where the plastic hinge is expected to form) as the HR specimen T1, computed according to Eurocode 3 (CEN 2003) provisions.

The numerical results for both specimens T1 and Weld_T1 are compared in Figs. 10 and 11. In terms of overall behavior, the connections clearly yield different responses. Bolt fracture determines the collapse of all T-stubs. Comparison of the $F-\Delta$ responses of the welded specimens shows that as the weld throat thickness increases, the stiffness and resistance improve but the deformation capacity significantly decreases (Fig. 10). It should be noted that the increase of a_w leads to a decrease of m . To determine the influence of welding itself, comparisons have to be made between specimen T1 and Weld_T1(iii) that have similar values of the distance m . Clearly, if the flange-to-web connection radius is replaced with a fillet weld, the stiffness and the resistance of the connection improve, but the deformation capacity is greatly reduced: it drops from a gap between flanges of 8.70 and 6.22 mm. For specimens T1 and Weld_T1(ii), the $F-\Delta$ curves are surprisingly coincident. However, in the welded case, the ductility is smaller. Table 2 sets out the main characteristics of the various $F-\Delta$ curves.

Regarding the bolt force and prying forces, their magnitude in relation to the applied load is higher for smaller weld throat thickness, in the case of the welded specimen for all courses of loading (Fig. 11). The location of the contact forces also changes with the increase of loading. For the welded specimen Weld_T1(i), with

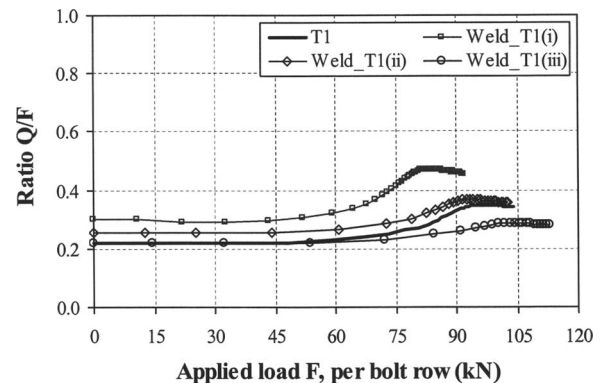


Fig. 11. Prying analysis for specimens T1 and Weld_T1

Table 2. Results for Various Examples (Values in Bold Correspond to Averaged Experimental Results; Underlined Values Include Web Deformation)

Speciman	Stiffness (kN/mm)			Strength (kN)		Δ_u	Q/F	
	$k_{e,0}$	$k_{pl,0}$	$k_{e,0}/k_{pl,0}$	K–R	F_u	(mm)	K–R	Ultimate resistance
T1	83.54	2.68	29.60	65–85	103.99	8.70	0.24	0.34
	49.00	1.73	28.32	58–87	102.81	9.49	—	—
P1	63.27	2.01	31.48	60–73	91.76	10.77	0.33	0.44
P2	117.06	3.49	33.54	70–100	116.72	6.18	0.18	0.25
P3	72.62	2.30	31.62	60–75	95.41	10.17	0.26	0.40
P4	97.86	4.24	23.08	70–103	115.97	4.68	0.20	0.26
P5	101.23	6.00	16.88	90–120	130.20	3.63	0.18	0.18
P6	76.56	2.36	32.44	55–75	95.53	10.06	0.26	0.42
P7	91.45	2.97	30.79	70–93	111.34	7.56	0.22	0.29
P9	128.47	6.19	20.76	85–120	131.43	3.31	0.13	0.16
P10	43.88	0.90	48.63	40–47	76.79	32.75	0.56	0.77
P11	122.80	6.82	18.01	90–110	121.15	2.94	0.20	0.21
P13	81.31	2.19	37.17	55–72	93.71	11.38	0.24	0.42
P14	81.97	1.07	76.69	45–65	86.57	24.15	0.24	0.53
P16	111.23	8.44	13.18	85–112	125.69	3.06	0.19	0.20
P17	138.31	3.86	35.81	115–165	192.01	9.29	0.22	0.36
P18	171.57	2.56	66.96	150–200	266.57	26.07	0.27	0.44
P24	80.46	1.89	42.51	65–87	108.14	13.80	0.24	0.31
P25	127.66	2.59	49.29	65–85	104.26	8.72	0.32	0.34
Weld_T1(i)	73.50	1.70	43.12	50–78	92.02	10.85	0.34	0.45
Weld_T1(ii)	88.04	2.51	35.07	60–87	102.75	8.01	0.27	0.36
Weld_T1(iii)	107.29	3.31	32.41	75–97	113.10	6.22	0.22	0.28
WT1	69.29	1.57	44.24	55–76	94.98	14.20	0.27	0.37
	71.09	2.09	34.01	58–69	183.83	14.33	—	—
WT4A	88.12	2.84	31.03	68–98	107.95	5.18	0.23	0.27
	86.96	4.37	19.90	70–98	103.26	4.33	—	—
WT7_M12	84.26	2.99	28.14	65–95	107.52	5.56	0.23	0.27
	91.18	3.78	24.12	60–96	100.64	4.44	—	—
WT7_M16	116.09	5.08	22.85	80–104	132.34	11.00	—	—
WT7_M20	137.70	5.61	24.54	88–118	145.72	8.77	—	—

smaller a_w , Q is located closer to the bolt axis than in the remaining specimens. With reference to the influence of the assembly type, Fig. 11 shows that in the elastic regime the ratios Q/F for specimens T1 and Weld_T1(iii) are coincident but as the load increases the same ratios decrease in the welded case. It is worth noting that even though T1 and Weld_T1(ii) yield identical $F-\Delta$ behavior, the evolution of Q/F with the course of loading is different (Fig. 11).

The difference in performance of the HP-T-stub T1 and the welded equivalents Weld_T1 is rather surprising. In terms of the overall deformation behavior, the differences can arise due to the redefinition of the length m that slightly increases in the welded case. This justifies the fact that stiffness and resistance also decrease. Regarding the deformation capacity the increase of the same distance m improves the ultimate deformation of the connection, Δ_u . With respect to the prying effect, the disparity of results was not expected.

Influence of Geometrical Parameters

This section highlights the influence of the T-stub geometry on the overall behavior. The graphs from Figs. 12 and Table 2

compare the $F-\Delta$ response of some HR-T-stub specimens with the original response (T1). The collapse condition of several specimens is determined by bolt tension fracture (black circles) or cracking of the flange (black square). The results show the following:

1. If the gauge of the bolts increases, consequently increasing the distance m between plastic hinges, the connection strength and stiffness decrease but the deformation capacity improves [Fig. 12(a)] (variation of the gauge of the bolts: specimens P1, $w=100$ mm, and P2, $w=80$ mm).
2. The enlargement of the pitch of the bolts and/or the edge distance implies larger T-stub widths and therefore higher stiffness and resistance values but reduced deformation capacity (Girão Coelho 2004) (variation of the pitch of the bolts: specimens P3, $p=30$ mm, P4, $p=65$ mm, P5, $p=80$ mm, P16, $p=70$ mm; variation of the edge distance: specimens P6, $e=15$ mm, P7, $e=25$ mm, and P16, $e=35$ mm).
3. As the flange thickness decreases, the component ductility improves considerably, while stiffness and resistance decrease; in this case, the flange-bolt stiffness decreases and, as

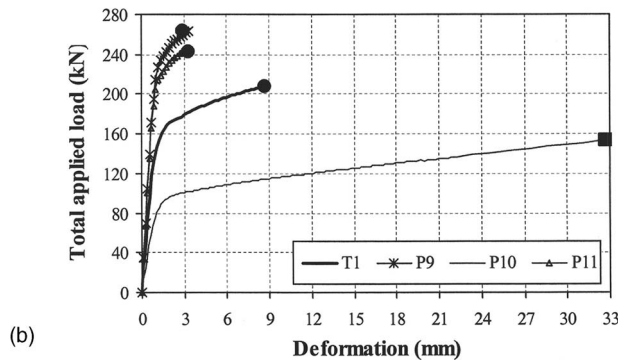
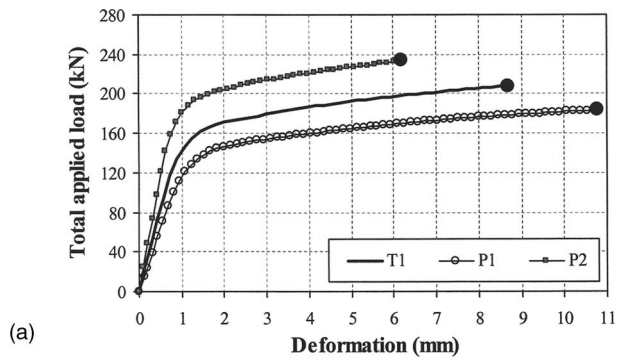


Fig. 12. Influence of geometrical distances on overall behavior (examples from HR-T-stub series): (a) gauge of bolts, w ; (b) flange thickness, t_f

a consequence, the degree of plastic deformation in the flange increases [Fig. 12(b)] (variation of the flange thickness: specimens P9, $t_f=14$ mm, P10, $t_f=7$ mm, and P11, $t_f=14$ mm).

Fig. 13 plots the numerical results obtained for specimen WT4A ($p=45$ mm; $e=30$ mm) against the experiments (Girão Coelho et al. 2004). The load-carrying behavior is traced in Fig. 13(a) showing good agreement of the results. Fig. 13(b) compares the numerical results for WP-T-stub specimens WT1 and WT4A. In both cases the bolt determines failure. In terms of overall behavior the conclusions drawn for specimen T1 and P16 are identical to this case. The comparison of the bolt experimental and numerical responses is shown in Fig. 13(c). The results are accurate despite the fact that the numerical prediction underestimates the bolt deformation capacity.

Finally, in order to assess the influence of the number of bolts, the numerical/experimental results for tests WT4A (two bolt-rows) and WT7_M12 (one bolt-row) are taken into account. These specimens are similar except for the number of bolts. The responses are identical though the specimen with only one bolt row shows improved ductility.

Influence of Bolt

Fig. 14(a) illustrates the influence of the bolt diameter on the overall behavior of HR-T-stubs (specimen P16, $\phi=12$ mm, specimen P17, $\phi=16$ mm, and specimen P18, $\phi=20$ mm). Essentially, if the bolt diameter is bigger, the initial stiffness, the strength, and the ductility improve greatly but the postlimit stiffness decreases. Also, for a given geometry, the bolt ceases to be the determining factor of collapse. The bolt-threaded length has an effect on the overall response if the bolt governs the specimen collapse. In

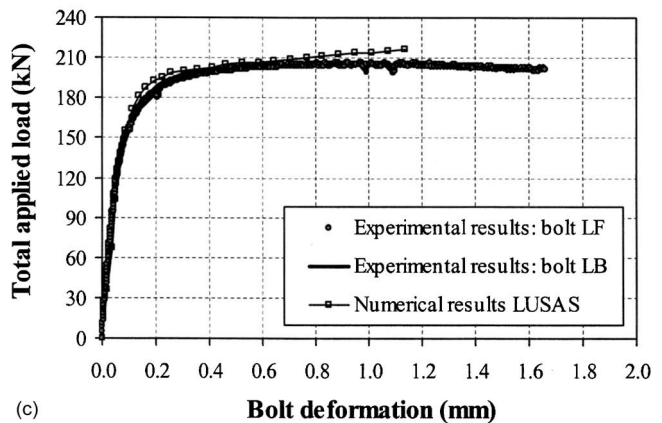
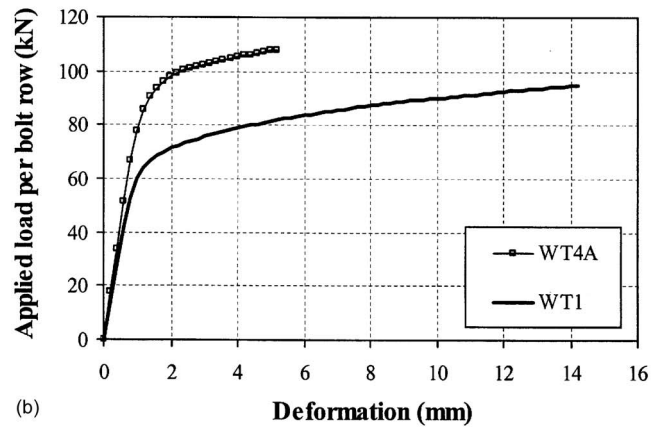
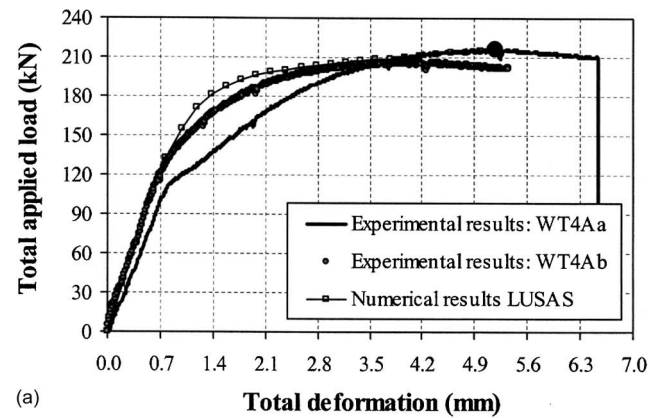


Fig. 13. Results for specimen WT4A: (a) load-carrying behavior; (b) influence of variation of pitch of bolts and edge distance on overall behavior (numerical results); and (c) bolt elongation behavior (experimental results shown correspond to broken bolts from specimen WT4Ab)

that case, if the threaded portion of the bolt is longer, the deformation capacity of the whole connection increases. The remaining properties do not change much [Fig. 14(b); specimen P25, full-threaded bolt]. The effect of the bolt preloading is the enhancement of the initial stiffness [Fig. 14(b); specimen P24, preloaded bolt]. Comparison of the behavior of the specimens with larger bolts (M16 and M20) confirms the previous considerations. This conclusion is also corroborated with experimental evidence (specimens from series WT7) (Girão Coelho et al. 2004).

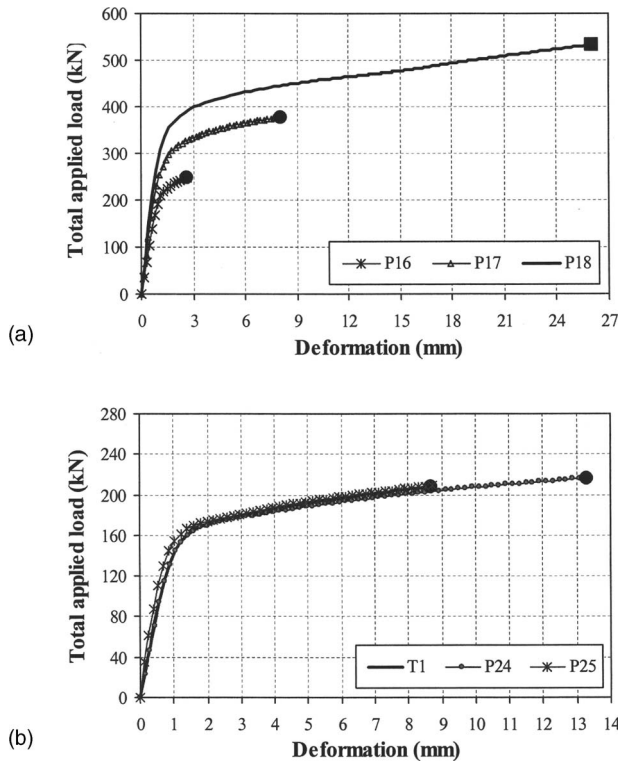


Fig. 14. Influence of bolt dimensions on overall behavior (examples from HR-T-stub series): (a) bolt diameter, ϕ and geometry from P16; (b) bolt thread length, L_{tg} and preloading, S_0

Influence of Flange Steel Grade

Regarding the effect of the flange steel grade, Fig. 15 shows that the initial stiffness is not affected by the steel properties (as long as the Young modulus is constant) but as the yield stress of the flange, $f_{y,f}$ increases resistance and postlimit stiffness also

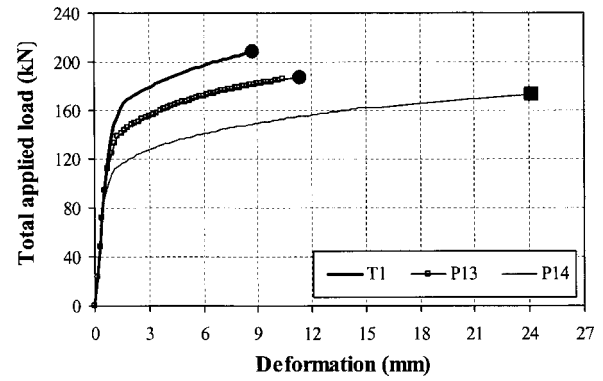


Fig. 15. Influence of flange steel grade on overall behavior

increase and deformation capacity decreases. Specimens P13 and P14 employ nominal S355 and S275, respectively.

Summary of Parametric Study

Table 2 summarizes the principal behavioral characteristics of the specimens from the parametric study. The main properties of the $F-\Delta$ curves are: (1) initial stiffness, $k_{e,0}$; (2) postlimit stiffness, $k_{pl,0}$; (3) full plastic strength, F_{Rd} ; (4) ultimate resistance, F_u ; and (5) deformation capacity, Δ_u . The values of F_{Rd} are not easy to define in this case and therefore are not reported in the table. Instead, the values indicated below the “K-R” column refer to the knee range of the curve, which corresponds to the transition from the stiff to the weak part of the $F-\Delta$ curve. The stiffness and strength values that appear in the table are computed per bolt row. The postlimit stiffness, $k_{pl,0}$, is evaluated by means of a regression analysis of the $F-\Delta$ postlimit response. Finally, Table 3 sets out the main conclusions drawn from the parametric study.

Table 3. Summary of Main Conclusions Drawn from Parametric Study (Notation: $x \uparrow \Rightarrow y \uparrow$ Means That If x Increases Then y Also Increases; Similarly, $x \uparrow \Rightarrow y \downarrow$ Means That If x Increases Then y Decreases)

	Strength		Stiffness		Ductility
	F_{Rd}	F_u	$k_{e,0}$	$k_{pl,0}$	Δ_u
(a) Assembly type					
	WP $\Rightarrow F_{Rd} \uparrow$	WP $\Rightarrow F_u \uparrow$	WP $\Rightarrow k_{e,0} \uparrow$	WP $\Rightarrow k_{pl,0} \uparrow$	WP $\Rightarrow \Delta_u \downarrow$
(b) Throat thickness (WP-T-stubs only)					
a_w	$a_w \uparrow \Rightarrow F_{Rd} \uparrow$	$a_w \uparrow \Rightarrow F_u \uparrow$	$a_w \uparrow \Rightarrow k_{e,0} \uparrow$	$a_w \uparrow \Rightarrow k_{pl,0} \uparrow$	$a_w \uparrow \Rightarrow \Delta_u \downarrow$
(c) Connection geometry					
w	$w \uparrow \Rightarrow F_{Rd} \downarrow$	$w \uparrow \Rightarrow F_u \downarrow$	$w \uparrow \Rightarrow k_{e,0} \downarrow$	$w \uparrow \Rightarrow k_{pl,0} \downarrow$	$w \uparrow \Rightarrow \Delta_u \uparrow$
p	$p \uparrow \Rightarrow F_{Rd} \uparrow$	$p \uparrow \Rightarrow F_u \uparrow$	$p \uparrow \Rightarrow k_{e,0} \uparrow$	$p \uparrow \Rightarrow k_{pl,0} \uparrow$	$p \uparrow \Rightarrow \Delta_u \downarrow$
e	$e \uparrow \Rightarrow F_{Rd} \uparrow$	$e \uparrow \Rightarrow F_u \uparrow$	$e \uparrow \Rightarrow k_{e,0} \uparrow$	$e \uparrow \Rightarrow k_{pl,0} \uparrow$	$e \uparrow \Rightarrow \Delta_u \downarrow$
t_f	$t_f \uparrow \Rightarrow F_{Rd} \uparrow$	$t_f \uparrow \Rightarrow F_u \uparrow$	$t_f \uparrow \Rightarrow k_{e,0} \uparrow$	$t_f \uparrow \Rightarrow k_{pl,0} \uparrow$	$t_f \uparrow \Rightarrow \Delta_u \downarrow$
(d) Bolt characteristics					
ϕ	$\phi \uparrow \Rightarrow F_{Rd} \uparrow$	$\phi \uparrow \Rightarrow F_u \uparrow$	$\phi \uparrow \Rightarrow k_{e,0} \uparrow$	$\phi \uparrow \Rightarrow k_{pl,0} \downarrow$	$\phi \uparrow \Rightarrow \Delta_u \uparrow$
L_{tg}	— ^a	— ^a	— ^a	— ^a	$L_{tg} \uparrow \Rightarrow \Delta_u \uparrow$
S_0	— ^a	— ^a	$S_0 \uparrow \Rightarrow k_{e,0} \uparrow$	— ^a	— ^a
(e) Plate material					
	$f_{y,f} \uparrow \Rightarrow F_{Rd} \uparrow$	$f_{y,f} \uparrow \Rightarrow F_u \uparrow$	— ^a	$f_{y,f} \uparrow \Rightarrow k_{pl,0} \uparrow$	$f_{y,f} \uparrow \Rightarrow \Delta_u \downarrow$

^aNo influence.

Conclusions

The T-stub model is widely accepted as a simplified model for the characterization of the behavior of the tension zone of a bolted joint, which constitutes the most important source of deformability of the whole connection.

The use of partial strength joints is becoming increasingly common but their design requires greater care since the ductility demand is much higher. The evaluation of the deformation capacity of single T-stubs is therefore very important since it covers one of the brittle components of bolted joints, the bolt in tension/bending. Current design specifications based on the T-stub model rely on pure plastic yield line mechanisms and the estimation of the level of prying forces (which increase the bolt force) results from one-dimensional elastic models that overlook some important phenomena. An extrapolation to failure conditions on these grounds is hardly justifiable.

The numerical investigation presented in this paper provides accurate deformation predictions (up to failure) of the T-stub response. Particular emphasis on the characterization of the T-stub failure modes and corresponding ductility levels is given. According to Eurocode 3 (CEN 2003) there are three possible models of failure of an equivalent T-stub: (1) mode 1: complete yielding of the flange; (2) mode 2: bolt failure with yielding of the flange; and (3) mode 3: bolt failure. The occurrence of a given collapse mode depends on the relation between the flexural resistance of the flanges and axial resistance of the bolts. The computation of these parameters is based on pure plastic conditions since the material strain hardening effect is not accounted for in the design code (CEN 2003). Furthermore, no limits are imposed to the ductility of connections that mainly depend on material ductility (bolt and flange) and structural discontinuities (welds, bolt holes, etc.). The assessment of the latter property is linked to the attainment of ultimate conditions, i.e., cracking of material. Concerning these ultimate conditions, four possible failure (fracture) mode typologies are proposed: (1) type-11, characterized by a plastic type-1 mode and cracking of the flange material at ultimate conditions [e.g., specimen P18, Fig. 14(a)]; (2) type-13, also a type-1 plastic mechanism but with fracture of the bolt at limit conditions [e.g., specimen P17, Fig. 14(a)]; (3) type-23, where the plastic mode involves both flange and bolt and the deformation capacity is governed by the bolt itself [e.g., specimen P16, Fig. 14(a)]; and (4) type-33, a type-3 plastic mode and deformation capacity determined by bolt fracture. Each fracture mode exhibits different ductility properties as clearly shown in the comparative graphs of Fig. 14(a), for instance. Previous research from Bursi and Jaspart (1997), Zajdel (1997), Wanzeck and Gebbeken (1999), and Swanson et al. (2002) was focused on single examples. Consequently, no conclusions on the ductility performance of connections could be drawn. Bursi and Jaspart (1997) and Zajdel (1997) proposed a model for a type-13 T-stub (T1, also analyzed above). Wanzeck and Gebbeken (1999) considered two T-stubs (P1K and P2K), both corresponding to a type-11 fracture mode. Swanson et al. (2002) analyzed a specimen failing according to a type-23 fracture mode.

This research work covers all possible failure modes and highlights the parameters affecting the deformation capacity of bolted T-stubs and their influence on the overall behavior of the connection has been qualitatively and quantitatively assessed. The next logical step forward is the provision of design rules concerning this topic. In addition, the numerical three-dimensional model

allows the evaluation of the prying forces, thus opening the way to more reliable design rules that prevent brittle failure of the T-stub, as detected in some cases.

Finally, the authors are currently developing a simplified analytical model that looks promising in assessing the failure of the steel joints.

Acknowledgments

Financial support from the Portuguese Ministry of Science and Higher Education (Ministério da Ciência e Ensino Superior) under contract grants from PRODEP and FCT (Grant No. SFRH/BD/5125/2001) for Ana M. Girão Coelho is gratefully acknowledged.

References

- American Institute of Steel Construction (AISC). (2005). "Single unified structural steel code for steel buildings." Chicago (in preparation).
- Astaneh, A. (1985). "Procedure for design and analysis of hanger-type connections." *Eng. J.*, 22(2), 63–66.
- Bursi, O. S., and Jaspart, J. P. (1997). "Benchmarks for finite-element modeling of bolted steel connections." *J. Constr. Steel Res.*, 43(1), 17–42.
- European Committee for Standardization (CEN). (2003). "Eurocode 3: prEN 1993-1-8: 20xx, Part 1.8: Design of joints." *Eurocode 3: Design of steel structures, Stage 49*, Brussels, Belgium.
- Gebbeken, N., Wanzeck, T., and Petersen, C. (1997). "Semi-rigid connections, T-stub model-Report on experimental investigations." *Rep. No. 97/2*, Institut für Mechanik und Static, Univ. des Bundeswehr München, Munich, Germany.
- Gioncu, V., Matescu, G., Petcu, D., and Anastasiades, A. (2000). "Prediction of available ductility by means of local plastic mechanism method: DUCTROT computer programme." *Moment resistant connections of steel frames in seismic areas: Design and reliability*, F. Mazzolani, ed., Spon, London, 95–146.
- Girão Coelho, A. M. (2004). "Characterization of the ductility of bolted end plate beam-to-column steel connections." Ph.D. dissertation, Univ. of Coimbra, Coimbra, Portugal.
- Girão Coelho, A. M., Bijlaard, F., Gresnigt, N., and Simões da Silva, L. (2004). "Experimental assessment of the behaviour of bolted T-stub connections made up of welded plates." *J. Constr. Steel Res.*, 60, 269–311.
- Kato, B., and McGuire, W. (1973). "Analysis of T-stub flange-to-column connections." *J. Struct. Div. ASCE*, 99(5), 865–888.
- LUSAS 13.3. (2000). *Theory manual, Version 13.3*, Finite Element Analysis Ltd, Surrey, U.K.
- Nair, R. S., Birkemoe, P. C., and Munse, W. H. (1974). "High strength bolts subject to tension and prying." *J. Struct. Div. ASCE*, 100(2), 351–372.
- Packer, J. A., and Morris, L. J. (1977). "Discussion of a limit state design method for the tension region of bolted beam-to-column connections." *J. Struct. Div. ASCE*, 104(9), 1546.
- Piluso, V., Faella, C., and Rizzano, G. (2001a). "Ultimate behavior of bolted T-stubs. I: Theoretical model." *J. Struct. Eng.*, 127(6), 686–693.
- Piluso, V., Faella, C., and Rizzano, G. (2001b). "Ultimate behavior of bolted T-stubs. II: Model validation." *J. Struct. Eng.*, 127(6), 694–704.
- Swanson, J. A. (1999). "Characterization of the strength, stiffness and ductility behavior of T-stub connections." Ph.D. dissertation, Georgia Institute of Technology, Atlanta.
- Swanson, J. A., Kokan, D. S., and Leon, R. T. (2002). "Advanced finite-element modeling of bolted T-stub connection components." *J. Constr. Steel Res.*, 58, 1015–1031.

- Thornton, W. A. (1985). "Prying action—A general treatment." *Eng. J.*, 22(2), 67–75.
- Vasarhelyi, D. D., and Chiang, K. C. (1967). "Coefficient of friction in joints of various steel." *J. Struct. Div. ASCE*, 93(4), 227–243.
- Virdi, K. S. (1999). "Guidance on good practice in simulation of semi-rigid connections by the finite element method." *Numerical Simulation of Semi-Rigid Connections by the Finite Element Method, COST C1, Rep. of Working Group 6—Numerical Simulation*, K. S. Virdi, ed., Brussels, Belgium, 1–12.
- Wanzek, T., and Gebbeken, N. (1999). "Numerical aspects for the simulation of end plate connections." *Numerical Simulation of Semi-Rigid Connections by the Finite Element Method COST C1, Rep. of Working Group 6—Numerical Simulation*, K. S. Virdi, ed., Brussels, Belgium, 13–31.
- Weynand, K., Jaspert, J. P., and Steenhuis, M. (1995). "The stiffness model of revised Annex J of Eurocode 3." *Connections in Steel Structures III; Proc. 3rd Int. Workshop on Connections*, R. Bjorhovde, A. Colson, and R. Zandonini, eds., Trento, Italy, 441–452.
- Yee, Y. L., and Melchers, R. E. (1986). "Moment-rotation curves for bolted connections." *J. Struct. Eng.*, 112(3), 615–635.
- Zajdel, M. (1997). "Numerical analysis of bolted tee-stub connections." *TNO-Rep. No. 97-CON-R-1123*.
- Zoetemeijer, P. (1974). "A design method for the tension side of statically loaded bolted beam-to-column connections." *Heron*, 20(1), 1–59.